ADVANCED FUNCTIONAL MATERIALS
www.afm-journal.de

Ortho- vs *Bay*-Functionalization: A Comparative Study on Tetracyano-Terrylenediimides

Glauco Battagliarin, Sreenivasa Reddy Puniredd, Sebastian Stappert, Wojciech Zajaczkowski, Suhao Wang, Chen Li, Wojciech Pisula, and Klaus Müllen**

In this paper n-type semiconductors synthesized via selective fourfold cyanation of the *ortho*- and *bay*-positions (2,5,10,13- and 1,6,9,14-positions respectively) of teyrrylenediimides are reported. A detailed study about the impact of the diverse functionalization topologies on the optoelectronic properties, self-organization from solution, solid-state packing, and charge carrier transport in field-effect transistors is presented. The *ortho*-substitution preserves the planarity of the core and favors high order in solution processed films. However, the strong intermolecular interactions lead to a microstructure with large aggregates and pronounced grain boundaries which lower the charge carrier transport in transistors. In contrast, the well-soluble *bay*-functionalized terrylenediimide forms only disordered films which surprisingly result in n-type average mobilities of 0.17 cm^2/Vs after drop-casting with similar values in air. Processing by solvent vapor diffusion enhances the transport to 0.65 cm^2/Vs by slight improvement of the order and surface arrangement of the molecules. This mobility is comparable to highest n-type conductivities measured for solution processed PDI derivatives demonstrating the high potential of TDI-based semiconductors.

1. Introduction

Terrylenediimide (TDI) is the higher homologue of perylenediimide (PDI) in the series of rylenediimides.[1] Similar to PDIs, TDIs possess high thermal, chemical and photochemical stability, combined with large electron affinities.[2] Variation of their imide substituents can be used to influence the solid-state packing, while core functionalization allows one to tune the electronic and optical properties. While PDIs are one of the most investigated materials for n-type semiconductors,[3] TDI based systems have been only marginally explored.[4] Nevertheless TDIs offer distinct advantages since their elongated scaffold allows multiple functionalization and induces a higher tendency to π–π stacking.[5] This, in turn, can be beneficial for high charge carrier mobilities, especially in solution processed active films.[6]

Dr. G. Battagliarin, Dr. S. R. Puniredd, S. Stappert, W. Zajaczkowski, Dr. S. Wang, Dr. C. Li, Dr. W. Pisula, Prof. Dr. K. Müllen
Max Planck Institute for Polymer Research
Ackermannweg 10, 55128 Mainz, Germany
E-mail: pisula@mpip-mainz.mpg.de; muellen@mpip-mainz.mpg.de

DOI: 10.1002/adfm.201401573

In this work we investigate the impact of the selective fourfold cyanation of the *ortho*- and *bay*-positions (2,5,10,13- and 1,6,9,14-positions respectively, **Scheme 1**) on TDIs. More precisely this paper is intended to 1) compare the reactivity of the *ortho*- and *bay*-positions and the impact of the diverse functionalization topologies on the optoelectronic properties and 2) study the influence of the different geometries on the self-organization from solution, solid-state packing and charge carrier transport in field-effect transistors.

Synthetically, *bay*-functionalization can be regarded as the historical and more established core modification of rylenediimides, mainly realized via direct halogenation and further substitution.[7] *ortho*-Functionalization represents the youngest synthetic method in ryleneimide chemistry, selectively achieved via metal catalyzed reactions.[8] A major difference between *ortho*- and *bay*-substitutions is their impact on molecular geometry, solubility and solid-state packing. In fact the steric interaction between the *bay*-substituents and the residual *bay*-hydrogens leads to a twisting of the conjugated system which is prone of reducing aggregation,[9] while *ortho*-functionalization preserves the planarity of the core even in the case of sterically demanding substituents.[8a,b,d,e] While planarity is believed to favor solid-state packing, some reports have demonstrated that the use of twisted molecules may be also applied to achieve high mobilities.[10]

2. Procedure

2.1. Synthesis

The synthesis of two tetracyano-terrylenediimides starts from the common precursor **TDI**, as shown in Scheme 1. This derivative has been previously investigated as n-type semiconductor, showing moderate n-type as well as p-type mobilities, despite the presence of the bulky imide substituents.[4c] In this case it has been chosen as core structure and starting point of the synthesis due to its good solubility. Selective *ortho*-functionalization is achieved via the ruthenium catalyzed reaction earlier published by our group to give the 2,5,10,13-tetraboronate ***o*-bor-TDI** in good yields.[8d] Successive conversion into the

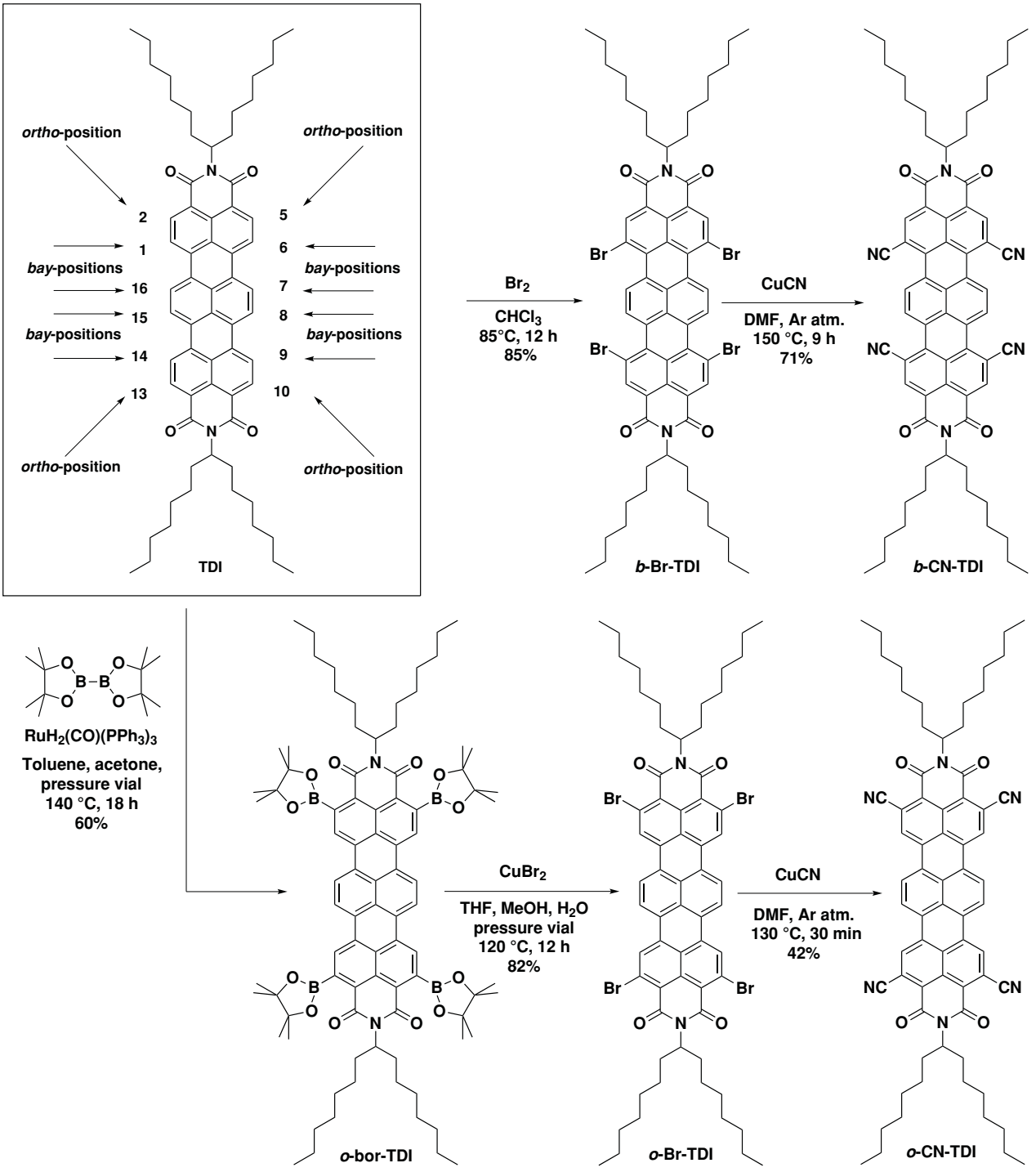

Scheme 1. Schematic explanation of *ortho*- and *bay*- positions of terrylenediimides (inset) and synthetic routes to ***b*-CN-TDI** (upper side) and ***o*-CN-TDI** (lower side).

tetrabromo derivative ***o*-Br-TDI** using copper(II) bromide is preferred to the direct conversion of boronates into nitriles due to the higher reaction yields and the easier purification.[8]f The 1,6,9,14-substituted ***b*-Br-TDI** is, instead, synthesized via nucleophilic bromination in high yields. The Rosenmund von Braun cyanation using copper(I) cyanide is applied to the two brominated isomers. Shorter times and lower temperatures are required for the *ortho*-derivative as compared to the *bay*-isomer. It must be noted that the cyanation of ***o*-CN-TDI** proceeds in very high yields, however, the extreme insolubility of the material leads to major losses during purification.

The introduction of the cyano substituents strongly enhances the tendency to aggregation with different consequences for the two functionalization patterns: the planar *ortho*-substituted

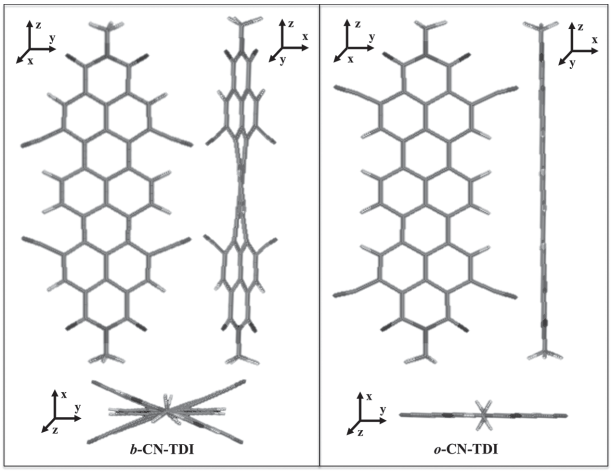

Figure 1. DFT-calculated geometries of N-methyl substituted *ortho*- and *bay*-tetracyano TDIs.

***o*-CN-TDI** exhibits poor solubility at room temperature (lower than 1 mg/mL) even in chloroform and o-dichlorobenzene, in which the twisted ***b*-CN-TDI** appears fairly soluble (7 mg/mL). This behavior can be understood considering the expected impact of the substitution patterns on the molecular geometries, also confirmed by the calculated structures of the two systems (**Figure 1**): while ***o*-CN-TDI** appears to be completely planar, favoring strong π–π interaction, ***b*-CN-TDI** possesses a twisted core, with each naphthalene fragment being distorted of an angle of about 15 ° in respect to the neighboring one.

2.2. Characterization

Optical characterization of the two cyano-derivatives by UV–Visible absorption spectroscopy and fluorescence spectroscopy reveals a bathochromic shift in the absorption and emission for both derivatives as compared to unsubstituted TDI (**Table 1**, **Figure 2**). The red-shift is slightly more accentuated for the *ortho*-substituted system, while all derivatives show comparable absorptivities.

The electrochemical properties of ***b*-CN-TDI** and ***o*-CN-TDI** have been investigated via cyclovoltammetric measurements (**Table 2**). While core unsubstituted TDIs are known to undergo a double electrochemical reduction at the same potential, the introduction of cyano substituents removes the degeneracy, showing two distinct reduction peaks for both derivatives (Figure S1, Supporting Information).[2b] Additionally, in the range of potentials investigated ***o*-CN-TDI** appears to undergo a third reduction at −2.01 V, not observed for ***b*-CN-TDI**. The LUMO and HOMO levels of the two isomers, estimated from the electrochemical measurements and the optical bandgap, respectively, appear substantially lowered in energy compared to the parent unsubstituted **TDI** (having a LUMO in the range between −3.5 and −3.7 eV and HOMO between −5.2 and −5.4 eV).[4c] The variation in energy levels between both substitution patterns is only minor, with the *bay*-substituted derivative possessing a slightly higher electron affinity as compared to the *ortho*-isomer. Despite the slight variations in the absolute values, DFT-calculations also predict similar energies for the HOMO and LUMO levels of the two derivatives (Table 2). Therefore, differences between the compounds in the affinity towards an electron transport in the transistor are not expected.

Table 1. Optical properties of tetracyanated terrylenediimides and of TDI, for direct comparison.

TDI[a]	ε [$M^{-1}cm^{-1}$][b]	λ_{max} [nm]	λ_{em} [nm][c]
TDI	1.27×10^5	651	669
***b*-CN-TDI**	1.12×10^5	657	673
***o*-CN-TDI**	1.48×10^5	661	680

[a]Optical properties measured in chloroform; [b]measured at λ_{max}; [c]excited at λ = 632 nm.

2.3. Self-Assembly and Device Performance

Based on the above reported results, the new TDIs appear as suitable candidates for use as n-type semiconductors in field effect transistors. Their charge carrier transport properties are studied in bottom-gate, bottom-Au contact FETs with a hexamethyldisilazane (HMDS) SiO_2 dielectric. In the first step, both TDIs are deposited by drop-casting a 5 mg/mL chlorobenzene solution on FET substrates heated at 100 °C in nitrogen atmosphere, followed by annealing at 250 °C for 1 h. It has to be emphasized that the solubility of the compounds significantly differs as mentioned earlier. Therefore, additional thermal treatment is necessary to completely dissolve ***o*-CN-TDI** at the same concentration as ***b*-CN-TDI**. Expectedly, pronounced differences in device performance between both compounds are observed. Under nitrogen conditions, ***b*-CN-TDI** leads to electron average mobilities of 0.17 $cm^2/Vs \pm 0.015$ cm^2/Vs with on/off ratio of 5×10^3 (**Figure 3**). The values in air after 24hr remain on an identical level with 0.11 cm^2/Vs. On one hand, the deep LUMO level of ***b*-CN-TDI** is supposed to favor electron injection from the Au electrode as suggested by the low threshold voltage of around 0 V. On the other hand, the nonlinear rise of the current at low source-drain voltage in the output curves is indicates trapping at the dielectric interface or/and high contact resistance (Figure 3a). To rule out interfacial problems, top-gate devices were fabricated by spin-coating ***b*-CN-TDI** and a subsequent PMMA dielectric on top of the active layer. Due to the fast solvent evaporation leading to molecular disorder an electron mobility of only 6×10^{-3} cm^2/Vs is determined (Figure S2, Supporting Information). More importantly, a similar nonlinear trend of the source-drain current is measured as for the bottom-gate transistor. This outcome points towards a charge injection barrier at the electrodes, which may be related to molecular disorder (see below the structural investigation by GIWAXS). This effect has been well described for pentacene grown on gold electrodes modified by various alkanethiol self-assembly monolayers to control the ordering and microstructure.[11] In contrast, ***o*-CN-TDI** shows no FET response using the same processing conditions. A field effect can be observed instead when a diluted chloroform solution of ***o*-CN-TDI** is concentrated by controlled evaporation and drop-casted. However only

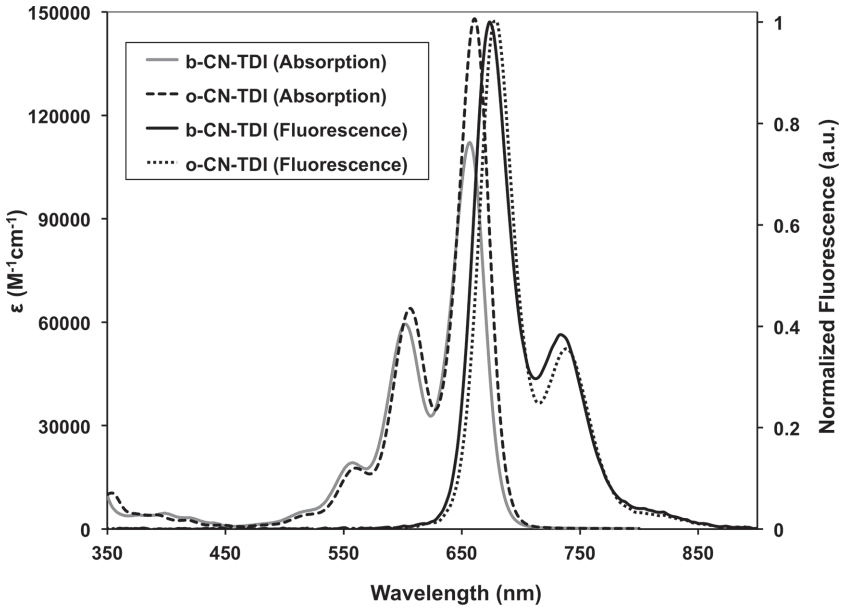

Figure 2. Direct comparison of the normalized absorption and emission spectra of ***o*-CN-TDI** and ***b*-CN-TDI** in chloroform (λ_{ex} = 632 nm for both compounds).

moderate maximum n-type performance of 10^{-3} cm^2/Vs and 1×10^2 on/off ratio can be measured for these films (Figure S3, Supporting Information). It has to be noted that these devices do not show a complete saturation in the output FET curves, in comparison to the clear saturation exhibited by ***b*-CN-TDI** suggesting intrinsic charges in the material or vicinity of the dielectric interface, as already observed for dicyano-NDIs.[12]

To understand the discrepancy in device behavior between ***b*-CN-TDI**, with an electron mobility up to 0.18 cm^2/Vs, and ***o*-CN-TDI** with only 10^{-3} cm^2/Vs, the supramolecular organization in the films is investigated by grazing incidence wide-angle X-ray scattering (GIWAXS). The patterns indicate large variations in packing mode of the molecules. Surprisingly, despite the low solubility after casting from both solvents chlorobenzene (**Figure 4**a) and chloroform (Figure S4, Supporting Information) ***o*-CN-TDI** reveals a pattern with well defined, intensive reflections which are characteristic for highly ordered molecules on the surface. Based on these results a model for the organization has been derived. Reflections on the meridional plane of the pattern (along q_z at $q_{x,y}$ = 0 Å^{-1}) are related to layers which are arranged parallel to the substrate. The main reflection and its higher order ones (h00) are assigned to an interlayer distance of 2.02 nm. This distance is in agreement with the spacing between lamellas containing TDIs, which are tilted with respect to the surface (surface organization is illustrated in Figure 4b). Scattering intensities on the equatorial and off-equatorial planes of the pattern are ascribed to the molecular packing within the layers. The off-equatorial reflections correspond to a tilting towards the layer axis, which is typical for crystalline disc-shaped molecules.[13] A π-stacking distance of 0.34 nm and a tilting angle of 50° in respect to the surface are determined from the off-equatorial reflection with the highest intensity. The arrangement of ***o*-CN-TDI** on the surface is illustrated in Figure 4b. This organization is in agreement with the bulk organization as found by two-dimensional wide-angle X-ray scattering (2DWAXS) on extruded, macroscopically aligned fibers (Figure S5, Supporting Information). The 2D pattern indicates also highly crystalline layer structure in which the TDI molecules are tilted. ***o*-CN-TDI** is not packed in a helical manner as observed earlier for other TDI derivatives, but the cores seem to be shifted along the long molecular axis (Figure 4b).[5] Because of steric reasons the *ortho*- and *bay*-cyano substitution might not allow a rotation of the aromatic cores towards each other, while a lateral shift induces a close packing by overcoming these constraints. TDIs without cyano substituents perform a rotation towards each other in order to overcome the steric hindrance of the branched side chains.[5]

In strong contrast to the pronounced surface order of ***o*-CN-TDI**, the GIWAXS pattern of ***b*-CN-TDI** shows a high number of quite isotropic reflections implying crystallinity, but low degree of preferential orientation of crystallites with respect to the substrate (Figure 4c). This means that the molecules are packed in domains, which are oriented relatively randomly towards the surface. Due to this lack of preference for a specific orientation and pronounced long-range disalignment a detailed structure analysis is not possible. The first main intensity scattering intensity related to the interlayer spacing is located at an identical position as for ***o*-CN-TDI**. Furthermore, it is possible to identify a reflection, which corresponds to the π-stacking of 0.35 nm. To conclude the GIWAXS analysis, both compounds are crystalline, but ***o*-CN-TDI** organizes on the surface in more defined way than ***b*-CN-TDI**. This is surprising since an enhanced charge carrier transport is observed for the latter TDI

Table 2. Electrochemical properties and theoretical and experimantal values of the frontier moleculr orbitals of tetracyano TDIs.

TDI	E_{red1} [V][a)]	E_{red2} [V][a)]	E_g [V][b)]	$LUMO_{exp}$ [eV][c)]	$HOMO_{exp}$ [eV][d)]	$LUMO_{calc}$ [eV][e)]	$HOMO_{calc}$ [eV][e)]
***b*-CN-TDI**	–0.47	–0.63	1.81	–4.33	–6.14	–4.49	–6.53
***o*-CN-TDI**	–0.54	–0.73	1.80	–4.26	–6.06	–4.45	–6.42

[a)]Half-wave potentials, determined by cyclic voltammetric measurement in 0.1 M solution of Bu_4NPF_6 in CH_2Cl_2: vs Fc/Fc^+; [b)]Optical bandgap, calculated from the optical absorption data; [c)]Estimated vs vacuum level from E_{LUMO} = –4.80 eV – E_{red1}; [d)]Estimated from HOMO = LUMO – E_g; [e)]Calculated using density functional theory as described in the Supporting Information.

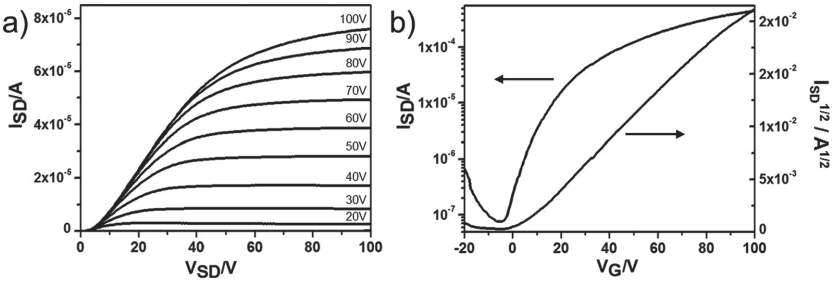

Figure 3. Field-effect transistor performance of ***b*-CN-TDI** drop-cast from a 5 mg/mL chlorobenzene solution a) output characteristics at various gate biases V_G and b) transfer curves at a source-drain bias of V_{SD} = 100 V.

derivative, which is highly misaligned. Generally, long-range organization favors the charge carrier transport, while a high density of grain boundaries and molecular disorder increase trapping and lower the device performance.

Microstructure describes the microscopic appearance of the compounds on the length scale between few hundred nanometers to few tens of micrometers. For the films of ***b*-CN-TDI** and ***o*-CN-TDI** both processed from chlorobenzene the microstructure is inspected by confocal microscopy since atomic force microscopy is not applicable due to the high roughness of the drop-cast inhomogeneous layers (**Figure 5**). ***o*-CN-TDI** shows a significantly larger surface roughness consisting of large aggregates in comparison to the relatively smooth film of ***b*-CN-TDI**. This difference in microstructure can be related to the variation in solubility between both TDI derivatives. Due to the limited solubility of ***o*-CN-TDI**, aggregates are probably formed already in solution and precipitate on the surface during casting. Although, the ***o*-CN-TDI** molecules are well organized as indicated by the above discussed GIWAXS data, distinct grain boundaries between the aggregates act as serious trapping sites for charge carriers and lead finally to a lack of any field-effect response.

To induce molecular order for the films of ***b*-CN-TDI**, solvent vapor diffusion (SVD) is applied on bottom-gate, bottom-contact HMDS modified devices. This processing method permits to control the self-assembly of the molecules on the surface during solvent evaporation and adjusts during this processes a balance between dewetting effects and various interactions.[14] Thereby, a drop of a dichlorobenzene solution is exposed to a saturated vapor of the same solvent in an airtight container. After the solvent is evaporated, long-range aligned, continuous films are obtained with improved saturated electron mobility up to 0.65 cm^2/Vs (average of 0.55 cm^2/Vs) and on/off ratio of 2.5×10^4 under nitrogen conditions (Figure S6, Supporting Information). The huge contact barrier observed already for the drop-cast films of ***b*-CN-TDI** is even more pronounced for these devices (Figure S6a, Supporting Information) as confirmed by the increase of the threshold voltage and the lack of saturation. The increase in mobility can be attributed to the fiber alignment along the transistor channel as one factor, which is considered to be beneficial for the charge carrier transport (Figure S7, Supporting Information). The driving force for the alignment is probably the difference of the surface energy between the gold electrodes and dielectric surface.[15] The second reason for the enhanced device performance is the higher molecular order as evident from the GIWAXS pattern for the SVD obtained film (Figure 4d). The shape of the reflections changes from isotropic for the drop cast layer to more distinct for the SVD film. The analysis of the pattern indicates an identical organization of ***b*-CN-TDI** as determined for the drop-cast ***o*-CN-TDI**. Thereby, the molecules are also assembled into layers and are tilted by ca 55° towards the surface. The π-stacking of 0.35 nm remains unchanged in comparison to the drop-cast layer. However, the crystallinity of SVD processed ***b*-CN-TDI** is significantly lower than that of ***o*-CN-TDI**

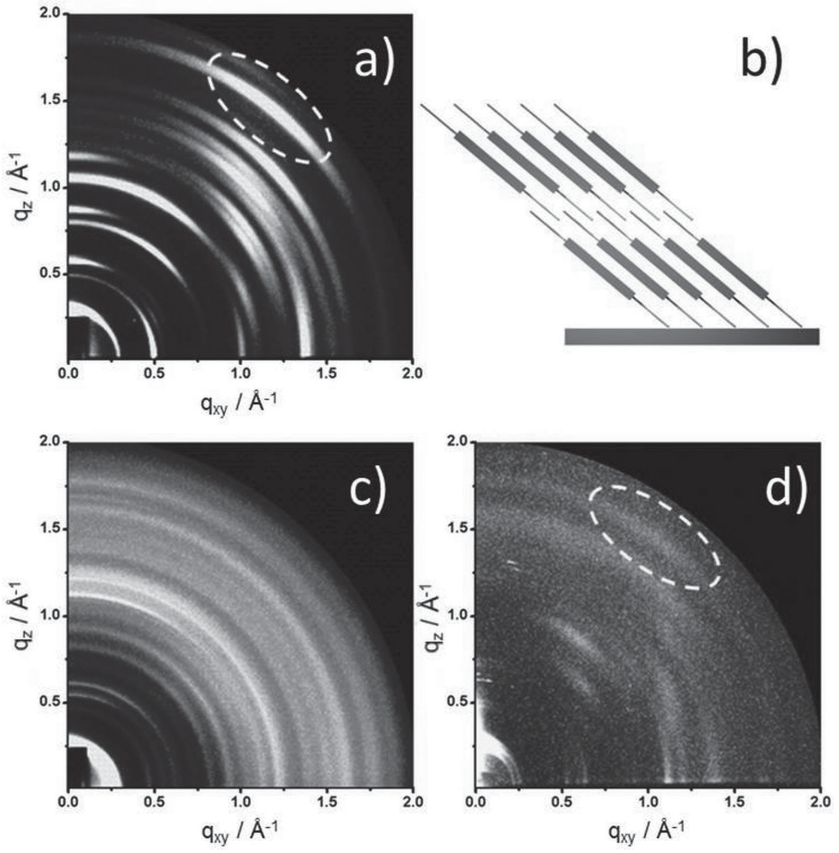

Figure 4. GIWAXS of a) ***o*-CN-TDI** (drop-cast from chlorobenzene), b) schematic illustration of the surface arrangement of ***o*-CN-TDI** after drop-cast from chlorobenzene; c) ***b*-CN-TDI** (drop-cast from chlorobenzene), d) SVD processed ***b*-CN-TDI**. Dashed circle indicates the π-stacking reflection.

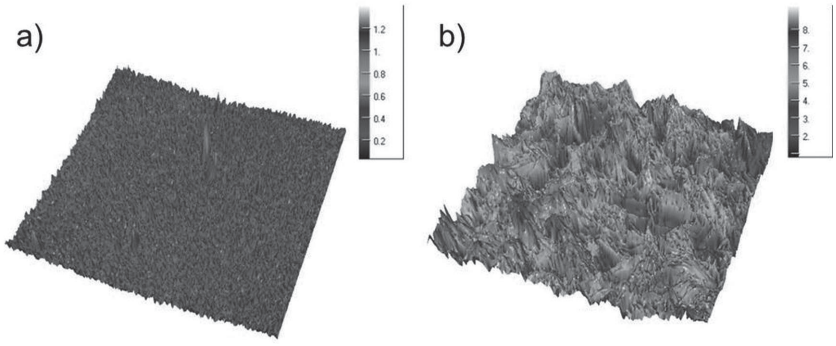

Figure 5. Confocal 3D topographic images of a) ***b*-CN-TDI** and b) ***o*-CN-TDI** after drop-casting from 5 mg/mL chlorobenzene. Both film height scales are in µm.

as obvious from the lack of higher order scattering intensities and larger FWHM (full width at half maximum) of the reflections.

3. Conclusions

In conclusion, two new tetracyano TDI were synthesized and studied in order to understand the effect of different substitution patterns. *ortho*- and *bay*-Functionalization show a similar impact on the electro-optical properties and energy levels of TDI, whereas a substantial difference in solubility, self-organization and solid-state packing is observed. While *ortho*-tetracyanation preserves the planarity of the core and appears to be beneficial for obtaining highly ordered solid-state films, the resulting microstructure with pronounced grain boundaries as trapping sites between the large aggregates is unfavorable for the charge carrier transport. On the other hand, the *bay*-functionalization guarantees solubility and despite the quite disordered organization in the thin film leads to n-type mobilities as high as 0.65 cm^2/Vs under inert atmosphere using ***b*-CN-TDI**. Such value is comparable to highest n-type mobilities measured for solution processed PDI derivatives,[16] demonstrating the high potential of TDI-based semiconductors.

This work underlines the importance of the molecular design, more specifically of the substitution pattern, on solubility and thus processability, which are both required for the film formation. Intuitively, it could be expected that the non-planar, poorly ordered ***b*-CN-TDI** afford a lower performance than the well-organized ***o*-CN-TDI**. Thus, the choice between the *ortho*- and *bay*-substitution positions has only minor impact on the electron poor character of the molecules, but tremendous consequences for the creation of charge trapping grain boundaries. Nevertheless, it is believed that long-range order is an essential requirement for further improvement of the TDI-based organic semiconductors. Consequently, in the future targeted engineering of the imide substituents will be explored to further improve the n-type performance of solution processed tetracyano-TDIs. More precisely, for the *bay*-functionalized derivative, β- and γ-branched alkyl substituents will be introduced to favor long-range order. For the *ortho*-derivative better solubilizing groups will be screened, such as longer alkyl chains, to reduce aggregation in solution and improve the microstructure.

4. Experimental Section

Unless otherwise noted, all reagents were obtained from commercial suppliers (e.g., Acros, Aldrich, Fluka, Strem). N,N′-Bis(1-heptyloctyl)-terrylene-3,4:11,12-tetracarboxylic acid diimide (**TDI**) has been synthesized following the procedure reported in the literature.[5] Preparative column chromatography was performed on silica gel 60 (0.063–0.2 mm/70–230 mesh ASTM) from Machery Nagel. Preparative gel permeation chromatography was carried out on Bio-Beads S-X1 Beads (200–400 Mesh) from BIO-RAD. ^{1}H and ^{13}C NMR spectra were recorded on a Bruker Avance 500 spectrometer and a Bruker Avance 250 spectrometer. Chemical shifts are denoted in δ unit (ppm), and were referenced to residual solvent. Infrared spectra were recorded on a Nicolet FT-IR 730 with an ATR unit (Zn-Se crystal). UV–Vis spectra in solution were recorded on a Perkin-Elmer Lambda 40 and a Perkin-Elmer Lambda 9 spectrometers. Fluorescence emission spectra were recorded on a J & M Tidas spectrometer. Elemental analysis of solid samples was carried out on a Foss Heraeus Vario EL.

*N,N′-Bis(1-heptyloctyl)-2,5,10,13-tetrakis[4,4,5,5-tetramethyl-1,3,2-dioxaborolan-2-yl]terrylene-3,4:11,12-tetracarboxylic Acid Diimide (**o-bor-TDI**)*: N,N′-Bis(1-heptyloctyl)-terrylene-3,4:11,12-tetracarboxylic acid diimide (0.80 g, 0.86 mmol) and bis(pinacolato)diboron (1.74 g, 6.84 mmol) are mixed together and dissolved in 60 mL anhydrous toluene and 2 mL anhydrous acetone. Argon is bubbled through the solution for 30 minutes. $RuH_2(CO)(PPh_3)_3$ (0.40 g, 0.43 mmol) is added to the mixture and the reaction is heated in a sealed pressure vial at 140 °C for 24 h. After cooling the system to room temperature, the solvent is evaporated and to the remaining liquid are added 400 mL methanol. The solid is filtered, dissolved in dichloromethane and precipitated once again in methanol. ***o-bor-TDI*** is obtained as dark blue solid with 60% yield (840 mg, 0.58 mmol). ^{1}H NMR (500 MHz, CD_2Cl_2) δ [ppm]: 8.74 (s, 4H, Ar-H), 8.53 (s, 4H, Ar-H), 5.19 – 4.99 (m, 2H, CH), 2.32 – 2.15 (m, 4H, CH_2), 1.95 – 1.75 (m, 4H, CH_2), 1.39 – 1.15 (m, 40H, C_nH_{2n}), 0.85 (t, J = 6.9 Hz, 12H, CH_3); ^{13}C NMR (126 MHz, 393 K, $C_2Cl_4D_2$) δ [ppm]: 165.4, 133.9, 131.0, 129.0, 128.1, 126.0, 125.7, 124.1, 123.8, 120.2, 84.1, 54.5, 32.4, 31.6, 29.2, 28.8, 26.6, 24.8, 22.3, 13.6; UV–Vis ($CHCl_3$): λ_{max} (ε): 663 nm (130 000 M^{-1} cm^{-1}), 608 nm (65 700 M^{-1} cm^{-1}), 563 nm (21 100 M^{-1} cm^{-1}); Fluorescence ($CHCl_3$, λ_{ex} = 632 nm) λ_{max}: 680 nm, 739 nm; ϕ_F: 1.00; HR-MALDI (ESI) *m/z* ($[M + H]^+$) calcd for $C_{88}H_{119}B_4N_2O_{12}$, 1438.9057; found, 1438.9071.

*N,N′-Bis(1-heptyloctyl)-2,5,10,13-tetrabromo-terrylene-3,4:11,12-tetracarboxylic Acid Diimide (o-Br-TDI) (**o-Br-TDI**)*: N,N′-Bis(1-heptyloctyl)-2,5,10,13-tetrakis[4,4,5,5-tetramethyl-1,3,2-dioxaborolan-2-yl] terrylene-3,4:11,12-tetracarboxylic acid diimide (0.40 g, 0.28 mmol) and $CuBr_2$ (0.75 g, 3.33 mmol) were suspended in 100 mL of a 8/1/1 mixture of dioxane/methanol/water and heated at 120 °C for 12 h in a sealed pressure vial. The reaction mixture was then cooled down, poured in 0.1 M HCl and filtered. The desired compound was obtained as a blue solid after column chromatography (silica, toluene) in 78% yield (0.27 g, 0.22 mmol). ^{1}H NMR (250 MHz, CD_2Cl_2) δ [ppm]: 8.41 (s, 4H, Ar-H), 8.10 (s, 4H, Ar-H), 5.25–5.04 (m, 2H, CH), 2.41–2.10 (m, 4H, CH_2), 2.10–1.85 (m, 4H, CH_2), 1.30 (m, 40H, C_nH_{2n}), 0.87 (t, J = 6.6 Hz, 12H, CH_3); ^{13}C NMR (126 MHz, CD_2Cl_2) δ [ppm]: 161.3, 134.0, 132.9, 129.6, 129.5, 128.9, 127.5, 124.4, 124.1, 120.3, 56.3, 32.9, 32.5, 30.2, 29.9, 27.9, 23.3, 14.5; UV–Vis ($CHCl_3$): λ_{max} (ε): 640 (152 000 M^{-1} cm^{-1}), 588 nm (82 300 M^{-1} cm^{-1}), 563 nm (21 100 M^{-1} cm^{-1}), 545 nm (26 900 M^{-1} cm^{-1}); Fluorescence ($CHCl_3$, λ_{ex} = 632 nm): 654 nm, 713 nm; ϕ_F: 0.89; Anal. calcd for $C_{64}H_{70}Br_4N_2O_4$: C 61.45, H 5.64, N 2.24; found: C 61.28, H 5.92, N 2.40.

*N,N′-Bis(1-heptyloctyl)-1,6,9,14-tetrabromo-terrylene-3,4:11,12-tetracarboxylic Acid Diimide (**b-Br-TDI**)*: N,N′-Bis(1-heptyloctyl)-terrylene-3,4:11,12-tetracarboxylic acid diimide (1.50 g, 1.60 mmol) was dissolved in 620 mL chloroform. Successively 17 mL of bromine were added to

the solution and the reaction was heated in exclusion of light for 12 h. After cooling the reaction to room temperature, 400 mL of a saturated solution of Na_2SO_3 were added and, after stirring the mixture for 30 min, the phases were separated. The organic solution was then dried over anhydrous magnesium sulfate and afterwards solvent was evaporated. The desired product was separated from the three times brominated TDI derivative by dissolving the solid in 200 mL of dichloromethane and afterwards precipitating it by addition of petrol ether (300 mL) and methanol (200 mL). The process was repeated until the triply brominated derivative was completely removed (monitored via TLC, SiO_2, toluene). The desired product was obtained as a dark blue solid (1.71 g, 1.37 mmol, 85% yield). ^{1}H NMR (500 MHz, 373 K, $C_2D_2Cl_4$) δ [ppm]: 9.56 (s, 4H, Ar-H), 8.95 (s, 4H, Ar-H), 5.19 (m, 2H, CH), 2.42–2.13 (m, 4H, CH_2), 2.05–1.85 (m, 4H, CH_2), 1.58–1.25 (m, 40H, C_nH_{2n}), 0.92 (s, br, 12H, CH_3); ^{13}C NMR (126 MHz, CD_2Cl_2) δ [ppm]: 162.6 137.9, 133.5, 131.1, 129.8, 129.0, 127.3, 126.3, 121.9, 120.1, 55.1, 32.3, 31.6, 29.2, 28.9, 26.8, 22.3, 13.7; UV–Vis ($CHCl_3$): λ_{max} (ε): 651 nm (87 500 $M^{-1}cm^{-1}$), 599 nm (48 600 M^{-1} cm^{-1}); Fluorescence ($CHCl_3$, λ_{ex} = 632 nm): 683 nm; ϕ_F: 0.79; Anal. calcd for $C_{64}H_{70}Br_4N_2O_4$: C 61.45, H 5.64, N 2.24; found: C 61.35, H 5.55, N 2.25.

*N,N′-Bis(1-heptyloctyl)-2,5,10,13-tetracyano-terrylene-3,4:11,12-tetracarboxylic Acid Diimide (**o-CN-TDI**)*: *N,N′*-Bis(1-heptyloctyl)-2,5,10,13-tetrabromo-terrylene-3,4:11,12-tetracarboxylic acid diimide (70 mg, 56 µmol) and copper(I) cyanide (0.10 g, 1.12 mmol) were mixed together and suspended in 20 mL anhydrous DMF in argon atmosphere. The reaction was heated at 130 °C for 30 min. After cooling the system to room temperature, 40 mL of saturated solution of ammonium iron(II) sulfate were added and the mixture heated to 60 °C for 2 h. After cooling to room temperature the solution was extracted with chloroform (3 × 80 mL), the organic phases were collected, extracted with brine (3 × 80 mL) and dried over magnesium sulfate. Chloroform was evaporated and the solid precipitating from the remaining solution was filtered and purified via column chromatography (silica, dichloromethane). The desired product was obtained as a dark blue solid with 42% yield (24 mg, 24 µmol). ^{1}H NMR (250 MHz, $C_2D_2Cl_4$) δ [ppm]: 8.89 (s, 4H, Ar-H), 8.77 (s, 4H, Ar-H), 5.19 (m, 2H, CH), 2.20 (m, 4H, CH_2), 1.98 (m, 4H, CH_2), 1.25 (m, 40H, C_nH_{2n}), 0.85 (m, 12H, CH_3); ^{13}C NMR (126 MHz, 373 K, *o*-dichlorobenzene-d_4) δ [ppm]: 191.2, 161.4, 135.9, 131.0, 130.2, 128.7, 127.9, 126.3, 125.2, 117.6, 117.5, 33.3, 32.5, 30.2, 29.9, 27.9, 23.2, 14.4; UV–Vis ($CHCl_3$): λ_{max} (ε): 661 nm (148 000 M^{-1} cm^{-1}), 607 nm (64 000 M^{-1} cm^{-1}), 560 nm (17 900 M^{-1} cm^{-1}); Fluorescence ($CHCl_3$, λ_{ex} = 632 nm): 680 nm, 739 nm; ϕ_F: 1.00; Anal. calcd for $C_{68}H_{70}N_6O_4$: C 78.89, H 6.81, N 8.12; found: C 78.54, H 6.47, N 8.01.

*N,N′-Bis(1-heptyloctyl)-1,6,9,14-tetracyano-terrylene-3,4:11,12-tetracarboxylic Acid Diimide (**b-CN-TDI**)*: *N,N′*-Bis(1-heptyloctyl)-1,6,9,14-tetrabromo-terrylene-3,4:11,12-tetracarboxylic acid diimide (0.43 g, 0.34 mmol) and copper(I) cyanide (0.62 g, 6.88 mmol) were suspended in 130 mL anhydrous DMF in argon atmosphere. The reaction was heated at 150 °C for 4 h. After cooling the system to room temperature, 120 mL of saturated solution of ammonium iron(II) sulfate were added and the mixture was heated to 60 °C for 2 hours. After cooling to room temperature the solution was extracted with chloroform (3 × 80 mL), the organic phases were collected and dried over magnesium sulfate. Successively chloroform was evaporated and the solution cooled down to room temperature. The precipitate was filtered and purified via column chromatography (silica, dichloromethane). The desired product was obtained as a dark blue solid with 70% yield (0.25 g, 0.24 mmol). ^{1}H NMR (500 MHz, 373 K, $C_2D_2Cl_4$) δ [ppm]: 9.88 (s, 4H, Ar-H), 9.07 (s, 4H, Ar-H), 5.21 (tt, J = 8.9, 6.0 Hz, 2H, CH), 2.38–2.21 (m, 4H, CH_2), 2.06–1.89 (m, 4H, CH_2), 1.46–1.23 (m, 40H, C_nH_{2n}), 0.92 (t, J = 6.9 Hz, 12H, CH_3); ^{13}C NMR (126 MHz, 373 K, $C_2D_2Cl_4$) δ [ppm]: 161.6, 137.8, 137.2, 130.7, 129.6, 128.8, 128.0, 126.5, 123.1, 118.8, 108.5, 55.8, 32.2, 31.5, 29.2, 28.9, 26.7, 22.3, 13.7; UV–Vis ($CHCl_3$): λ_{max} (ε): 661 nm (148 000 M^{-1} cm^{-1}), 607 nm (64 000 M^{-1} cm^{-1}), 560 nm (17 900 M^{-1} cm^{-1}); Fluorescence ($CHCl_3$, λ_{ex} = 632 nm): 680 nm, 739 nm; ϕ_F: 1.00; Anal. calcd for $C_{68}H_{70}N_6O_4$: C 78.89, H 6.81, N 8.12; found: C 78.85; H 6.74; N 8.02.

Molecular Modeling: The transport levels as well as the relative stabilities of the different conformers were determined via density functional calculations. For the ionization potential and the electron affinity first the geometry of the neutral as well as the charged states were optimized using the BP86-functional[17,18] in combination with a split-valence basis set (SV(P)) including polarization functions on all heavy atoms.[19] Energies were converged to an accuracy of 10^{-9} hartree, whereas the gradient norm was in the order of 10^{-4}. Single point calculations to determine the ionization potentials as well as the electron affinities at the optimized geometries of the charged and neutral species were performed on the BP86/TZVP level of theory including a solid state correction. Here we used a UPS/IEPS-calibrated version of the conductor like screening model (COSMO).[20] The turbomole program package[21] was used throughout.

Field-Effect Transistors: Bottom-gate, bottom-contact FETs were fabricated using substrates with a 200 nm thick SiO_2 dielectric covering highly doped Si acting as the gate electrode. The SiO_2 surface was functionalized with hexamethyldisilazane (HMDS) to minimize interfacial trapping sites. The channel lengths and widths are 20 and 1400 µm, respectively. All the electrical measurements are performed using Keithley 4200 SCS in a glovebox under nitrogen atmosphere. Top-gate transistors were prepard also on Si/SiO_2 substrate with thermal evaporation of 25 nm Au bottom contact and 5 nm Cr adhesion layer (shadow mask with channel dimensions of W = 1000 µm and L = 30 µm). The substrates were cleaned before film deposition. The active layer of ***b*-CN-TDI** was prepared under glovebox conditions by spin-coating from 5mg/mL chlorobenzene solution at 2k rpm and annealed at 250 °C for 2 h. Top-gate (Sigma-Aldrich, M_w = 225 000) PMMA dielectric was spin-coated from 50 mg/mL Butyl Acetate solution at 2k rpm (thickness 320 nm) and annealed at 150 °C for 3 h. Finally 90 nm thick Au gate electrode was deposited by thermal evaporation.

Grazing Incidence Wide Angle X-Ray Scattering: GIWAXS measurements were performed using a custom setup consisting of rotating anode X-ray source (Rigaku Micromax, operated at 42 kV and 20 mA), Osmic confocal MaxFlux optics and a three pin-hole collimation system (JJ X-ray). Samples on the top of approx. 1 cm × 1 cm silicon platelets were irradiated at the incident angle (αi) of 0.20°. Diffraction patterns were recorded on a MAR345 image plate detector.

Three-Dimensional Confocal Surface Measurements: The three-dimensional (3D) topography images were obtained by using a confocal surface measurement system from NanoFocus µSurf C.

Optical Microscopy: The optical images were obtained by using a Zeiss optical polarized microscope.

Two-Dimensional Wide Angle X-Ray Scattering: 2D-WAXS measurements were performed using a custom setup consisting of the Siemens Kristalloflex X-ray source (copper anode X-ray tube, operated at 35 kV/20 mA), Osmic confocal MaxFlux optics, two collimating pinholes (1.0 and 0.5 mm – Owis, Germany) and an antiscattering pinhole (0.7 mm – Owis, Germany). The patterns were recorded on a MAR345 image plate detector (Marresearch, Germany). The samples were prepared by filament extrusion using a custom-built mini-extruder.

Solvent Vapor Diffusion: A 25 mL ***b*-CN-TDI** dichlorobenzene solution (concentration 3 mg/mL) is drop-cast on a HMDS modified SiO_2 dielectric surface and exposed to an airtight container (50 mL) that is saturated with dichlorobenzene solvent vapor (with 5 mL dichlorobenzene in the container) at room temperature.

Supporting Information

Supporting Information is available from the Wiley Online Library or from the author.

Acknowledgements

The authors gratefully acknowledge the financial support from the DFG Priority Program SPP1355, the One-P large-scale project no.212311, and BASF SE. G.B. gratefully acknowledges the IMPRS Ph.D. program for the

economical support. S.R.P. gratefully acknowledges the ERC Advanced Grant NANOGRAPH (AdG-2010–267160). The authors thank Dr. Adam Kiersnowski for helpful discussion and technical support for GIWAXS and Dr. Christian Lennartz from BASF SE for the modelling experiments.

Received: May 15, 2014
Revised: August 24, 2014
Published online: September 29, 2014

[1] a) A. Herrmann, K. Müllen, *Chem. Lett.* **2006**, *35*, 978; b) T. Weil, T. Vosch, J. Hofkens, K. Peneva, K. Müllen, *Angew. Chem. Int. Ed.* **2010**, *49*, 9068; c) L. Chen, C. Li, K. Müllen, *J. Mater. Chem. C* **2014**, *2*, 1938.

[2] a) S. K. Lee, Y. Zu, A. Herrmann, Y. Geerts, K. Müllen, A. J. Bard, *J. Am. Chem. Soc.* **1999**, *121*, 3513; b) S. Mais, J. Tittel, T. Basché, C. Bräuchle, W. Göhde, H. Fuchs, G. Müller, K. Müllen, *J. Phys. Chem. A* **1997**, *101*, 8435; c) F. Nolde, J. Qu, C. Kohl, N. G. Pschirer, E. Reuther, K. Müllen, *Chem. Eur. J.* **2005**, *11*, 3959.

[3] a) X. Zhan, A. Facchetti, S. Barlow, T. J. Marks, M. A. Ratner, M. R. Wasielewski, S. R. Marder, *Adv. Mater.* **2011**, *23*, 268; b) C. Li, H. Wonneberger, *Adv. Mater.* **2012**, *24*, 613; c) C. Huang, S. Barlow, S. R. Marder, *J. Org. Chem.* **2011**, *76*, 2386; d) F. Würthner, M. Stolte, *Chem. Commun.* **2011**, *47*, 5109; e) H. Qian, F. Negri, C. Wang, Z. Wang, *J. Am. Chem. Soc.* **2008**, *130*, 17970; f) W. Yue, A. Lv, J. Gao, W. Jiang, L. Hao, C. Li, Y. Li, L. E. Polander, S. Barlow, W. Hu, S. Di Motta, F. Negri, S. R. Marder, Z. Wang, *J. Am. Chem. Soc.* **2012**, *134*, 5770.

[4] a) M. Petit, R. Hayakawa, Y. Shirai, Y. Wakayama, J. P. Hill, K. Ariga, T. Chikyow, *Appl. Phys. Lett.* **2008**, *92*, 163301; b) M. Petit, R. Hayakawa, T. Chikyow, J. P. Hill, K. Ariga, Y. Wakayama, *Org. Electron.* **2009**, *10*, 1187; c) C. Liu, L. Zhihong, H. T. Lemke, H. N. Tsao, R. C. Naber, Y. Li, K. Banger, K. Müllen, M. M. Nielsen, H. Sirringhaus, *Chem. Mater.* **2010**, *22*, 2120.

[5] F. Nolde, W. Pisula, S. Müller, C. Kohl, K. Müllen, *Chem. Mater.* **2006**, *18*, 3715.

[6] M. Funahashi, *Polym. J.* **2009**, *41*, 459.

[7] G. Seybold, G. Wagenblast, *Dyes Pigm.* **1989**, *11*, 303.

[8] a) S. Nakazono, Y. Imazaki, H. Yoo, J. Yang, T. Sasamori, N. Tokitoh, T. Cédric, H. Kageyama, D. Kim, H. Shinokubo, A. Osuka, *Chem. Eur. J.* **2009**, *15*, 7530; b) S. Nakazono, S. Easwaramoorthi, D. Kim, H. Shinokubo, A. Osuka, *Org. Lett.* **2009**, *11*, 5426; c) J. E. Bullock, M. T. Vagnini, C. Ramanan, D. T. Co, T. M. Wilson, J. W. Dicke, T. J. Marks, M. R. Wasielewski, *J. Phys. Chem. B* **2010**, *114*, 1794; d) G. Battagliarin, C. Li, V. Enkelmann, K. Müllen, *Org. Lett.* **2011**, *13*, 3012; e) T. Teraoka, S. Hiroto, H. Shinokubo, *Org. Lett.* **2011**, *13*, 2532; f) G. Battagliarin, Y. Zhao, C. Li, K. Müllen, *Org. Lett.* **2011**, *13*, 3399.

[9] a) P. Osswald, F. Würthner, *J. Am. Chem. Soc.* **2007**, *129*, 14319; b) F. Würthner, *Chem. Commun.* **2004**, *14*, 1564.

[10] a) Z. Chen, M. G. Debije, T. Debaerdemaeker, P. Osswald, F. Würthner. *Chem. Phys. Chem.* **2004**, *5*, 137; b) R. Schmidt, J. H. Oh, Y. Sun, M. Deppisch, A. M. Krause, K. Radacki, H. Braunschweig, M. Könemann, P. Erk, Z. Bao, F. Würthner, *J. Am. Chem. Soc.* **2009**, *131*, 6215; c) M. Gsänger, J. H. Oh, M. Könemann, H. W. Höffken, A. M. Krause, Z. Bao, Fr. Würthner, *Angew. Chem. Int. Ed.* **2010**, *49*, 740.

[11] P. Stoliar, R. Kshirsagar, M. Massi, P. Annibale, C. Albonetti, D. M. de Leeuw, F. Biscarini, *J. Am. Chem. Soc.* **2007**, *129*, 6477.

[12] B. A. Jones, A. Facchetti, T. J. Marks, M. R. Wasielewski, *Chem. Mater.* **2007**, *19*, 2703.

[13] W. Pisula, X. Feng, K. Müllen, *Adv. Mater.* **2010**, *22*, 3634.

[14] S. Wang, L. Dössel, A. Mavrinskiy, P. Gao, X. Feng, W. Pisula, K. Müllen, *Small* **2011**, *7*, 2841.

[15] J. A. Lim, W. H. Lee, D. Kwak, K. Cho, *Langmuir* **2009**, *25*, 5404.

[16] C. Piliego, D. Jarzab, G. Gigli, Z. Chen, A. Facchetti, M. A. Loi, *Adv. Mater.* **2009**, *21*, 1573.

[17] J. P. Perdew, *Phys. Rev. B* **1986**, *33*, 8822.

[18] A. D. Becke, *Phys. Rev. A* **1998**, *36*, 3098.

[19] A. Schäfer, H. Horn, R. Ahlrichs, *J. Chem. Phys.* **1992**, *9*, 2571.

[20] A. Klamt, *J. Phys. Chem.* **1995**, *99*, 2224.

[21] R. Ahlrichs, M. Bär, M. Häser, H. Horn, C. Cölmel, *Chem. Phys. Lett.* **1989**, *162*, 165.